On the heating of nano- and microparticles in process plasmas

H R Maurer, H Kersten

HAL Id: hal-00613284
https://hal.science/hal-00613284

Submitted on 4 Aug 2011

On the heating of nano- and microparticles in process plasmas

H.R. Maurer, H. Kersten

Institute of Experimental and Applied Physics, University of Kiel, Germany

Abstract

Determination and understanding of energy fluxes to nano- or microparticles, which are confined in process plasmas, is highly desirable because the energy balance results in an equilibrium particle temperature which may even initiate the crystallization of nanoparticles. A simple balance model has been used to estimate the energy fluxes between plasma and immersed particles on the basis of measured plasma parameters. Addition of molecular hydrogen to the argon plasma results in additional heating of the particles due to molecule recombination. The measured particle temperature is discussed with respect to appearing plasma-particle interactions which contribute to the particle's energy balance.

Introduction

Today, plasma technology is a key feature in many emerging industrial sectors like microelectronics, nanotechnology, optics, biological or medical engineering and many others, dealing with surface modification. Here, the energetic conditions at the surface of a substrate in processes like sputtering, plasma etching, thin film deposition or surface modification are crucial for the improvement of applications with respect to morphology, stoichiometry and process rates [1-5]. Hence, monitoring and controlling the constitutional parameters like gas pressure and composition or substrate temperature is essential for the design of the process conditions.

Beneath treating macroscopic wafers in plasmas, also the plasma-based synthesis and modification of nanoscopic or microscopic particles (powder) with specific properties offers a variety of new applications [6-14], which may involve the improvement of optical or mechanical properties for coatings [9,14], for sintering processes [10], disperse composite catalysts [6] or polymorphous solar cells [7,8].

For example, Roca y Cabarrocas et.al [7] described the optimization of PIN (positive intrinsic negative) solar cells produced by plasma enhanced chemical vapor deposition from silane–hydrogen mixtures. To increase the deposition rate, the discharge has been operated under plasma conditions close to powder formation, where silicon nanocrystals contribute to the

deposition of so-called polymorphous silicon thin films. The authors could show that the increase in deposition rate can be achieved via an accurate control of the plasma parameters, e.g. decreasing the ion energy by increasing the total pressure. By using silane–helium mixtures, they were able to to increase both the deposition rate and the solar cell's efficiency, as required for cost effective thin film photovoltaics [7].

Nanoparticles produced in low-temperature plasmas are often found with crystalline structure [37], suggesting rather high particle temperatures during synthesis. Surprisingly this even applies to particles of high-melting-point materials, even though the gas temperature in these plasmas is often close to room temperature and particles may reside in the plasma only for a short duration [15]. Mangolini et.al presented a numerical study of nanoparticle heating in plasmas through energetic surface reactions. They found that, under realistic plasma conditions, particle temperatures can exceed the gas temperature by hundreds of Kelvin [15].

The composition of reactive low-temperature plasmas, and specifically the hydrogen content, is a convenient control of the nanostructure growth. Recently, highly-controllable self-assembly of various nanostructures and their arrays (nanocones [16], carbon connections [17] or nanotips [18]) in hydrogen-containing plasma was demonstrated experimentally. Hydrogen has many important functions in surface processes, such as etching, heating, passivation or crystallization of amorphous materials [19]. An effective passivation of the dangling bonds at the surface of growing nanostructures and surface heating are the most important ones.

The opportunity of independently controlling the surface fluxes of energy and hydrogen-containing radicals, enabling selective control of the nanostructure heating and passivation, has been demonstrated in a previous paper [20]. *In situ* energy flux measurements revealed that even a small addition of H_2 to low-pressure Ar plasmas causes a dramatic increase in the energy deposition through H recombination at the surface. The heat release is quenched by a sequential addition of a hydrocarbon precursor while the surface passivation remains effective. Such selective control offers an effective mechanism for deterministic control of growth shape, crystallinity, and density of nanostructures in plasma-aided nanofabrication [20].

Similar studies, related to the gas temperature dependence of nucleation and growth processes of hydrocarbon nanoparticles in low pressure Ar/CH_4 rf-discharges, have been performed by Beckers and Kroesen et.al [21]. Measuring the electron density by microwave cavity resonance technique allowed them to monitor nucleation processes on short time scales (μs). On larger time scales, coagulation times and growth rates are determined by means of measuring the phase angle between rf-voltage and current in correlation with laser light

scattering. The experimental results have shown a significant gas temperature dependence of both powder nucleation and growth processes. Within the measured gas temperature range (*20–130°C*) the particle growth rate decreased by a factor of *~4*, while the coagulation time increased by a factor of *~6* with increasing gas temperature [21].

Particles in a plasma environment and the measurement of their temperature

If particles are injected or grown in a plasma, they can be confined due to the balance of several forces acting on them [22,23]. Commonly, particles and surfaces in plasmas tend to be negatively charged [23-35] due to the much larger mobility of plasma electrons compared to that of positive ions. As the temperature of electrons in non-thermal plasmas is significantly higher than that of heavy species, the collection of electrons is even more pronounced in cold plasmas. The charge (and the subsequently the Coulomb interaction) between particles strongly reduces agglomeration and coalescence [26,27]. This enables achieving much more narrow and well-defined particle size distributions by non-thermal plasmas compared to other thermal or aerosol processes.

Like the injected particles, also electrode and reactor walls are biased negatively with respect to the potential of the plasma. Thus, negatively charged particles are repelled by strong electric fields in the space charge sheath regions. This offers the opportunity to confine particles in a plasma reactor and to strongly reduce the diffusion losses to the reactor walls [28-31], which is an advantage compared to most other aerosol processes for particle generation [23,32].

In addition to charging, confined particles are also influenced by several energetic fluxes from and towards them. The electronic and energetic conditions at the surface of small particles in low pressure plasmas are affected by their size and geometry [36-39]. Quickly a balance is archieved [23,33,34], resulting in the establishment of an equilibrium temperature T_μ. Microparticles typically reach a stable temperature within tens of milliseconds [43], which is determined by the balance of energy exchange with its environment.

Especially for nanoparticles, the effect of radiation cooling is reduced due to their small size compared to the emitted wavelength. As a consequence, nanoparticles in nonthermal plasmas can be heated to rather high temperatures [35]. This selective nanoparticle heating may have a dramatic consequence for their morphology and crystallinity and is likely one of the main reasons for the formation of crystallites in nonthermal plasmas even if the gas temperature

remains close to room temperature. Such crystallites are often incorporated in composite materials [16]. Recently, U. Kortshagen reviewed the involved processes and effects of non-thermal plasma synthesis for nanocrystals in related topical review paper [23].

Several studies addressed the grain temperature, both theoretically [39-42] and experimentally [33,34,43-47]. For example, Daugherty and Graves measured the temperature-dependent decay time of the fluorescence of manganese activated magnesium fluorogermanate particles in a pulsed argon discharge during the plasma-off phase [43]. Swinkels at al. utilized Rhodamine-B dyed melamine-formaldehyde particles, and compared their temperature-dependent emission spectrum in the plasma to spectra from a calibration oven [47]. Oliver and Enikov measured the incandescent radiation from particles in a plasma jet, which of course is only possible at rather high particle temperatures above 1000 K [46]. A rather novel method for the measurement of particle temperatures utilizes temperature-sensitive spectral features of phosphor grains, which are excited by means of an external illumination source [33,44].

For a quantitative description of particle heating in plasma environment the energy fluxes have to be measured either by calorimetric probes [2,48] or by suitable microparticle probes [44]. Based on probe theory for such test particles, a calorimetric balance model can be established where the particle temperature occurs as an observable.

Energy balance of particles in a plasma

Microparticles, confined in the sheath of a plasma, are exposed to multi-species bombardment from neutrals, radicals, electrons and ions as well as to electromagnetic plasma irradiation. The kinetic energy of the impinging electrons and ions, as well as their recombination energy, contributes to the heating of the particle surface. Furthermore - depending on the plasma environment - other processes like latent heat release of deposited material, exothermic reaction processes or association energy from recombination of dissociated molecules can account for the heating of the particle.

The contribution from plasma irradiation can be assumed to be negligible in typical rf-discharges, and also the role of metastables, which has been benchmarked by Do et al. [49] to

be in the order of some $\mu \mathrm{Wcm}^{-2}$, is insignificant. In the case of argon and argon-hydrogen plasmas, the integral energy influx density J_{in} can thus be described as

$$J_{\mathrm{in}} = J_{\mathrm{e}} + J_{\mathrm{i}} + J_{\mathrm{rec}} + J_{\mathrm{ass}} , \qquad (1)$$

where J_{e}, J_{i}, J_{rec} and J_{ass} denote the kinetic energy release density of electrons and ions and the energy influx densities due to recombination of charge carriers and dissociated molecules, respectively.

Typically, due to its small heat capacity a microparticle reaches a stable temperature T_{μ} within tens of milliseconds [43]. Then, the integral energy influx density J_{in} is balanced by integral energy loss density J_{out} due to radiation and conduction to the environment [42,47]

$$J_{\mathrm{out}} = J_{\mathrm{rad}} + J_{\mathrm{cond}} . \qquad (2)$$

A scheme of the mentioned energy flux densities is sketched in fig. 1. Now the mentioned energy flux densities for particles in the sheath of an electropositive low pressure rf-discharge will be quantified by a simple model.
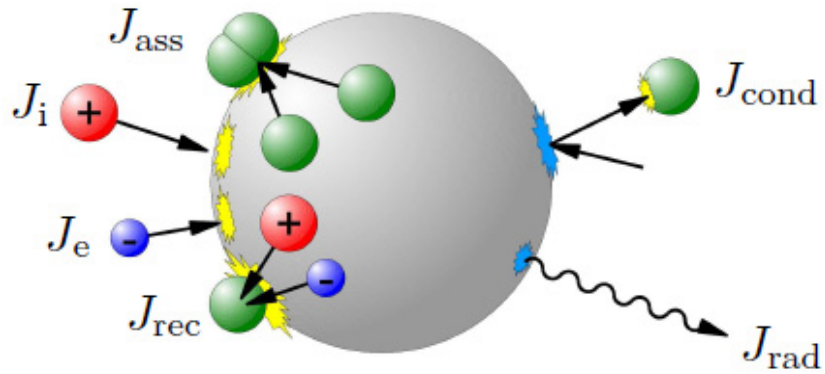

Figure 1:
Scheme of the energy flux densities between a microparticle and the surrounding plasma environment. The particle gains energy from the kinetic energy of electrons and ions, from their recombination and from reactive processes like the association of atoms at the particle surface. Energy loss occurs via conduction and radiation.

The electron influx density j_{e} towards a retarding surface at a yet unknown floating potential V_f is described by

$$j_{\mathrm{e}} = \alpha \frac{1}{4} n_{\mathrm{e},0} \exp\left\{\frac{V_f}{V_{\mathrm{e}}}\right\} \sqrt{\frac{8e_0 V_{\mathrm{e}}}{\pi m_{\mathrm{e}}}} \qquad (3)$$

where $n_{e,0}$ is the electron density in the undisturbed (bulk) plasma, m_e the electron mass, $V_e = k_B T_e/e_0$ the electron temperature in Volts, e_0 the elementary charge, T_e the electron temperature in Kelvin and k_B the Boltzmann constant. This description is valid for electrons with an isotropic Maxwellian electron energy distribution function (EEDF). The exponential term describes the reduction in n_e due to repulsion from the negatively charged microparticle surface and the root describes the mean electron thermal velocity. The duty cycle α is an approximation factor for the time-averaged electron density at a position z in the rf-sheath. It also includes the electron sticking coefficient. However, α will be named 'electron duty cycle' in the following for simplicity. The kinetic energy influx density due to electrons is then

$$J_e = j_e \cdot 2e_0 V_e. \qquad (4)$$

The factor $2e_0 V_e = 2k_B T_e$ is the mean kinetic energy of the electrons arriving at the particle surface. By contrast, for ions the particle is attractive, and the ion flux density j_i towards the particle is

$$j_i = \eta\, n_{e,0} \exp\{-0.5\} \sqrt{\frac{e_0 V_e}{m_i}} \cdot \left(1 - 2\frac{V_f}{V_e}\right)^{\beta} \qquad (5)$$

where the root describes the ion's velocity, which approaches sound (Bohm) velocity v_B at the sheath edge. Here the ion density at the sheath edge is described via the bulk electron density times a reduction factor, which accounts for the attenuation of ion density due to acceleration of the ions to v_B, and m_i denotes the ion mass. For impinging ions, the particles are assumed to be perfect absorbers in this description. The factor η accounts for the area of a two-dimensional projection of the object, as seen by the directed streaming ions. For a sphere, $\eta = 1/4$, for an ideal cylinder $\eta = 1/\pi$ and for a planar object facing towards the plasma volume $\eta = 1$. This equation is adopted from orbital motion limited (OML) probe theory [36]. In this theory, also a geometric OML correction factor is necessary, given in the brackets, where β again depends on the geometry. For an ideal plane probe $\beta = 0$, whereas for a small spherical microparticle $\beta = 1$. The kinetic energy influx density of ions is then given by

$$J_i = -j_i \cdot e_0 V_f. \qquad (6)$$

However, if the plasma consists of more than one kind of positive ions, e.g. in an argon-hydrogen mixture, the behavior of the different species has to be taken into account. In a multiple ion low pressure plasma with comparable ion densities $n_{i,k}$, each species marked with an index k enters the sheath with the bulk ion sound velocity [50]

$$v_B = \sqrt{\frac{e_0 V_e}{n_{e,0}} \sum_k \frac{n_{i,0,k}}{m_k}} \qquad (7)$$

and eqn. (5) has to be modified to

$$j_i = \sum_k j_{i,k} = \eta \sum_k n_{i,s,k} v_B \cdot \left(1 - 2\frac{V_f}{V_e}\right)^{\beta}$$
. (5a)

In this equation, $n_{i,s,k}$ is the ion density of species k at the sheath edge.

After hitting the particle, the ion can recombine at the particle surface. As the particle is not connected to an external electrical circuit, the involved electron has been collected by the particle from the plasma before, and the net work function is zero. Assuming that the recombination energy $E_{ion,k}$ is released to the particle, the energy influx density from recombination of a species k is

$$J_{rec} = \sum_k j_{i,k}(E_{ion,k} - E_{diss,k})$$
. (8a)

When the ions are molecular, such as H_3^+ or ArH^+, some energy might be required for their dissociation into stable atoms or molecules, which is considered in the term $E_{diss,k}$, and the ionization energy $E_{ion,k}$ (see table 1) of the ion resulting from the dissociative reaction is released. In a pure noble gas discharge with one ion species, eq. (8a) can simply be written as

$$J_{rec} = j_e E_{ion} ,$$
(8)

and the easier accessible j_e can be utilized instead of j_i due to the floating condition. Each ion-electron recombination on floating particles results in argon atom formation and the energy released in this case is equal to the ionization potential for Ar which is 15,76 eV.

An important energetic channel in molecular or reactive gases is the dissociation of molecules in plasma which occurs via electron neutral collisions. In low pressure plasmas the association process, where dissociated molecules recombine, most probably occurs on surfaces and, hence, on the surfaces of nano- or microparticles, too. The released energy from this process often plays an important role for the energy balance.

Again, Kortshagen investigated the production of silicon particles produced in silane plasmas which always have surface terminations with hydrogen [23]. In this case, dissociation processes and plasma chemistry occurs and the energetic interaction between plasma and microparticles has to account for energy release due to additional processes. An incident hydrogen radical can instantly react with a surface-bound hydrogen atom to form a hydrogen molecule. This process is called Rideal Eley mechanism. If there is no possibility for an incoming hydrogen radical to react with hydrogen at the particle surface, also two surface-bound atoms can recombine to form a hydrogen molecule, which is called Langmuir–Hinshelwood mechanism. When this molecule is released again, a net energy of 4,52 eV remains at the particle surface.

Assuming a Maxwellian velocity distribution of the gas atoms, the resulting energy flux density towards the particle can be estimated analogous to eq. (3) [47]

$$J_{\text{ass}} = \frac{1}{2}\Gamma_k\frac{1}{4}n_k\sqrt{\frac{8k_BT_{\text{gas}}}{\pi m_k}}E_{\text{diss,k}} \quad . (9)$$

In this equation, n_k is the number density of the dissociated gas species, 1/2 is the stoichiometric factor and the factor 1/4 accounts for the same geometric consideration as for the impinging electrons but without retarding potential. Γ_k is the association probability at the particle surface. For hydrogen the probability is expected to be $0.1 \ll \Gamma_H \leq 1$.

Table 1:
Specific constants of the most important species in an Ar-H_2 plasma [51-53]. The dissociation energies of the ions refer to the reactions $H_3^+ \rightarrow H_2 + H^+$ and $ArH^+ \rightarrow Ar + H^+$ [54,55].

	Ar	H_2	H	ArH^+	H_3^+
m [u]	39.9	2.0	1.0	40.9	3.0
E_{ion} [eV]	15.76	15.37	13.60	-	-
E_{diss} [eV]	-	4.52	-	4.02	4.37
γ	5/3	7/5	5/3	7/5	8/6

In summary, the integral energy influx density towards the particles described by eq. (1) is, thus, determined by the plasma parameters which can be measured, the electron duty cycle α, the gas mixture and occasionally by the release of energy at the surface due to association processes. Fig. 2 shows the dependence of the contribution of the sum of kinetic and potential energy of the impinging charge carriers to a plane area in dependence on α for a plasma with $V_e = 1$ eV and $n_{e,0} = 1 \cdot 10^{16}$ m^{-3}. Two cases are shown, the first one is an argon discharge and the second one a gas mixture of 90% argon and 10% hydrogen as modeled by Bogaerts et.al [56] for typical low-pressure discharge conditions. If the ion masses are comparable, J_i is weakly influenced by a change in the relative densities because v_B is not altered strongly. In an argon-hydrogen plasma, a drop in the relative fraction of the light ion population causes v_B to decrease. The contribution from kinetic ions to the integral energy influx is very small and, moreover, the ionization energies of different gases are often comparable.

However, if v_B is changed also V_f is affected and as a result also the J_e, J_i and J_{rec} are governed directly. Note, that the contribution J_{ass} is not shown in fig. 2 because only the effect of charge carriers should be demonstrated.
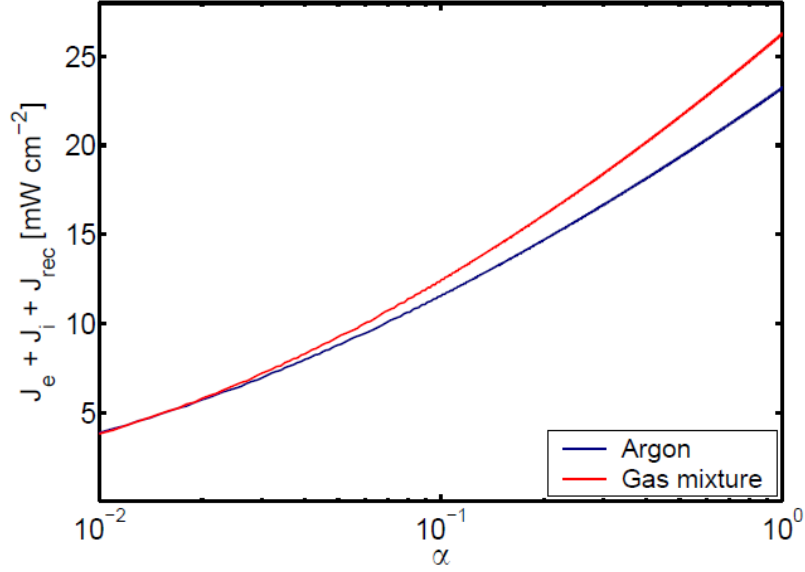
Figure 2:
Energy influx density towards a planar surface, facing towards the plasma volume due to the contribution of charge carriers, modeled for $V_e = 1\ eV$ and $n_{e,0} = 1 \cdot 10^{16}\ m^{-3}$ in argon as well as with an admixture of 10% hydrogen in dependence of the electron duty cycle α.

In thermal equilibrium of the particles trapped in the plasma, J_{in} is balanced by energy losses and eq. (2) is valid. The radiative energy loss density can be estimated from Stefan-Boltzmann's law

$$J_{rad} = \sigma \varepsilon_\mu \left(T_\mu^4 - T_{env}^4 \right) \tag{10}$$

where T_μ and T_{env} are the temperatures of the particles and the inner walls of the plasma chamber, respectively, ε_μ is the emissivity of the particles and σ is the Stefan-Boltzmann constant.

In low pressure conditions, the behavior of the gas molecules is described in the Knudsen regime [11, 12], where the energy loss density is linear in the gas pressure

$$J_{cond} = p_{gas} \frac{\gamma + 1}{16 (\gamma - 1)} \alpha_\mu \sqrt{\frac{8 k_B}{\pi m_{gas} T_{gas}}} (T_\mu - T_{gas}) \tag{11}$$

The adiabatic coefficient $\gamma = c_p / c_v$ for different gases is listed in table 1.

Example: fluorescent microparticles as thermal probes in an Ar/H₂ rf-plasma
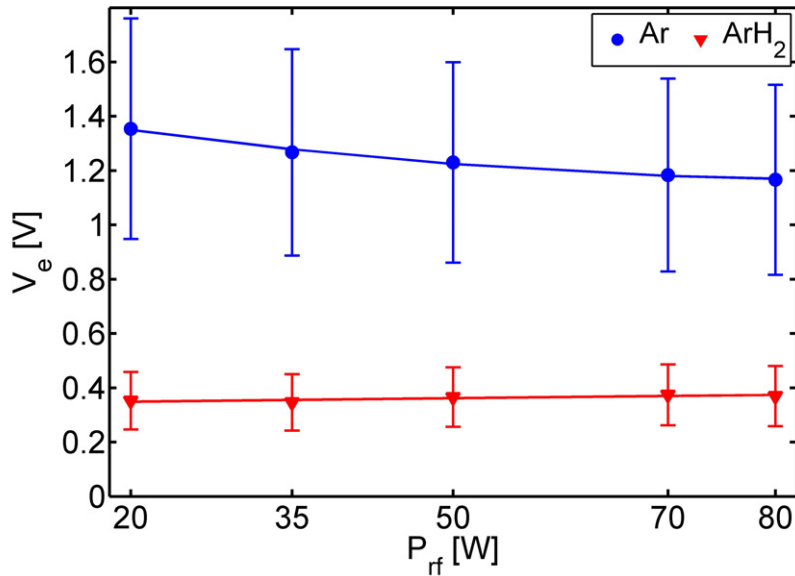

Figure 3:
Electron temperature as a function of rf power, determined by Langmuir Probe measurements at a total gas pressure of p_{gas} = 10 Pa. With respect to pure Ar, under admixture of 1 Pa H_2 the electron temperature drops by a factor less than 0.3. This behavior can be explained by inelastic electron-molecule collisions, involving vibrational and rotational electronic transitions. The error in this measurement is estimated to be up to 30%.
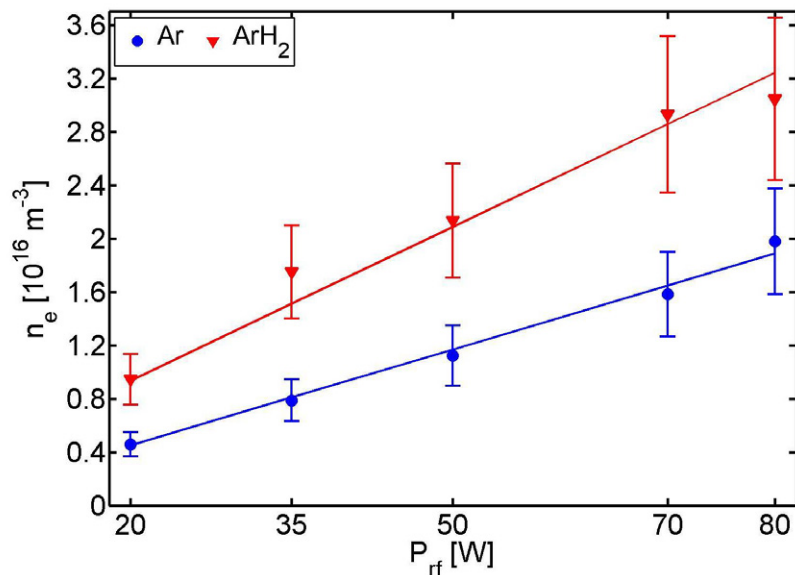

Figure 4:
Electron density, obtained by Langmuir Probe measurements at a total gas pressure of 10 Pa. Due to the more effective energy dissipation under the presence of molecular gas, the degree of ionization is increased by a factor of approximately 2 when H_2 is added. The accuracy of the measurements is estimated to be within 20%.
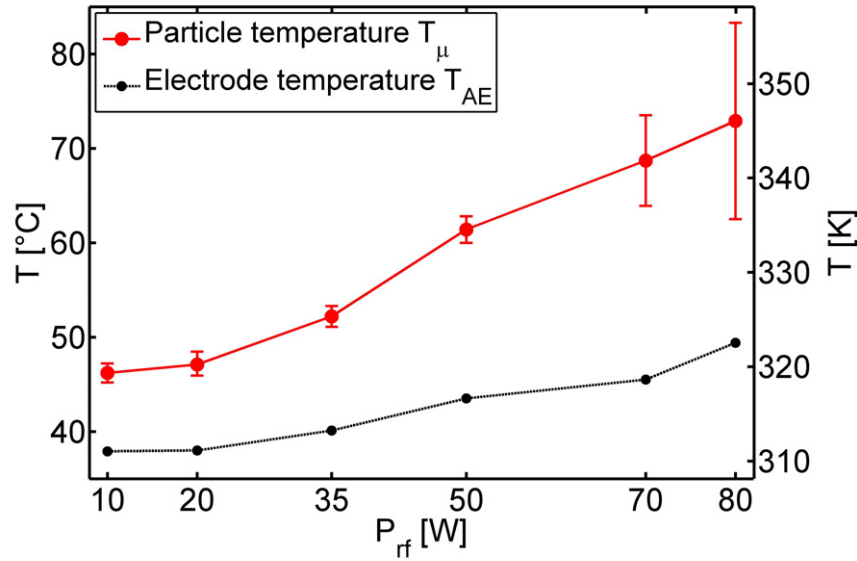
Figure5:
Particle temperatures T_μ and the corresponding temperatures of the Adaptive Electrode T_{AE}. The errors given for T_μ show the standard deviation of 10 subsequent measurements. At high discharge power, particle confinement becomes difficult, causing particle loss, a decreasing s/n ratio and increasing error bars. The error in T_{AE} is estimated to be below 0.5 K.

In principle, the model described above holds for nano-sized as well as for micro-sized particles. However, under comparable discharge conditions nanoparticles can become much hotter than microscaled particles. Nevertheless, the energy balance can be experimentally determined by suitable microparticles which are also heated to a certain extent and which can be easier handled.

As an example, the energy balance for microparticles which are confined in an argon-hydrogen rf-plasma in front of an Adaptive Electrode (AE) has been studied. The experimental setup (PULVA-INP) as well as the procedure for the measurement of the particle temperature by temperature-dependent fluorescence have been extensively described elsewhere [33,34]. The plasma parameters n_e and $V_{e,}$, measured by a Langmuir probe, show pronounced differences under admixture of molecular gas as depicted in figs. 3 and 4. At admixture of 10% molecular hydrogen the electron temperature is dramatically reduced and, in the same time, the electron density is nearly doubled. The measured particle temperatures T_μ in the argon-hydrogen mixture are given in fig. 5, together with the temperature of the Adaptive Electrode T_{AE} as a reference value.

The measurements regarding T_μ and T_{AE} have been aided by in-situ Tuning Diode Laser Absorption Spectroscopy (TDLAS) on the argon 810.4 nm emission line for determination of the gas temperature T_{gas} at the position of the particles. As in low pressure plasmas the

majority of recombination processes occur at surfaces, T_{gas} is expected to be smaller than T_μ. However, the measurement of T_{gas} by optical techniques with the accuracy desired for our requirements is rather difficult, especially in an rf-plasma where mechanical vibrations of vacuum pumps are present. Additionally, no spatial resolution is attained and the temperatures measured by TDLAS tend to be systematically too high due to the involved assumptions and, last but not least, due to technical restrictions like etaloning or jitter. It turned out that an estimation of T_{gas} based on T_μ and T_{AE} can be more suitable if T_μ and T_{AE} are comparable. For our calculations we estimated the gas temperature by $T_{gas} = \frac{1}{2}(T_\mu + T_{AE})$.

However, in gas mixture plasmas different ion species occur with different unknown densities. In the case of argon and hydrogen, three dominant ion species were observed by mass spectrometry [24,57] showing comparable densities: Ar^+, ArH^+ and H_3^+. Similar findings were obtained in the simulations, published by the group of Bogaerts et al. [56] for a 90% argon + 10% hydrogen rf-discharge at a pressure of 13.3 Pa. The relative ion densities at the sheath edge, required for the calculation of J_{in} are taken from this simulation.

The accommodation coefficient of the microparticles is estimated to be $\alpha_\mu \approx 0.86$ [34,47]. The emissivity is estimated to be $\varepsilon = 0,5$ [58]. However, especially for nanoparticles with diameters shorter than the emitted wavelength, ε is smaller and radiative cooling can be negligible compared to conductive cooling under typical discharge conditions [23,34].

The required electron duty cycle α has been determined by a comparison of J_{in} and J_{out} in pure argon, where α was treated as a free parameter [33]. Under the assumption that the vertical position z of the microparticles in the rf-sheath is not changed significantly by the addition of hydrogen, α should remain unchanged.

The total energy flux densities in the argon-hydrogen mixture, calculated on the basis of eqns. (1) – (8) and the discussed constants, are shown in fig. 6.
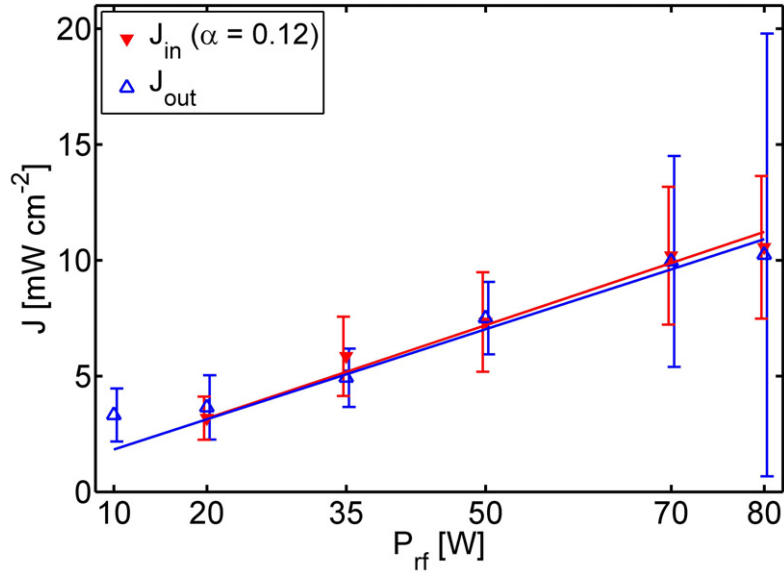
Figure6:
Total energy fluxes in the argon-hydrogen mixture, characterized in figs. 3 and 4. The duty cycle α has been obtained from a similar comparison in pure argon, treating α as an adjusting parameter. Here, the dissociation ratio $\Gamma_H n_H \sim n_e$ is treated as a free parameter to match energy influx and loss.

In this calculation, the product $\Gamma_H n_H$ was taken as a free parameter and was varied until a good accordance between J_{in} and J_{out} was achieved. As V_e is nearly constant within the considered parameter range and the hydrogen atoms are provided by electron impact dissociation, the number density n_H of atomic hydrogen can be expected to be proportional to the electron density n_e. At a value of $\Gamma_H n_H \approx 3 n_e$ a good agreement for J_{in} and J_{out} is found. The individual contributions to J_{in} and J_{out} are given in fig. 7. The resulting dissociation ratio

$$
\begin{aligned}
D \quad &:= \quad \frac{n_H}{n_H + 2 n_{H2}} \\
&\approx \quad \frac{3}{\Gamma_H} \cdot 10^{-4}
\end{aligned}
$$
(12)

is in the order of 10^{-3}, as the association possibility Γ_H is expected to be close to 1. This value for D is comparable to the results measured in a capacitively coupled rf-discharge by Pipa et al. [59] when extrapolated to a position close to the position of the confined particles near the electrode. However, the estimation of D is only a rough value, but its agreement to existing evidence can be seen as a confirmation. The contribution to J_{in} due to association processes is significant, as shown in fig. 7 and is approximately 20% of the total energy influx even close to the adaptive electrode. Inside the plasma volume it can be expected to become more dominant if no competitive association can occur at nearby surfaces.
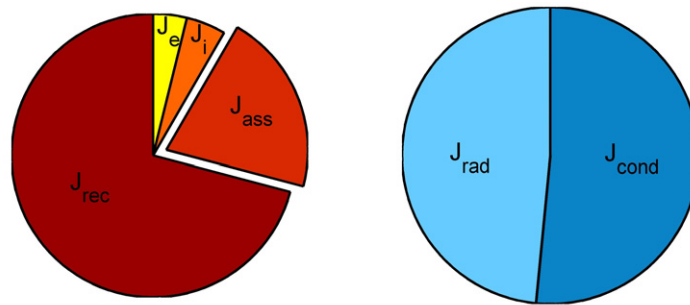
Figure 7:
Comparison of the different contributions to the total energy flux densities shown in fig. 6 for a 10 Pa Ar/H$_2$ discharge.
left: Contributions to the total energy influx density J$_{in}$ for an electron duty cycle of α = 0.12, calculated from the plasma parameters.
right: Contributions to the total energy loss density J$_{out}$, calculated from T$_\mu$

Conclusion

Determination and understanding of energy fluxes from process plasma to confined nano- or microparticles is highly desirable because the particles energy balance results in an equilibrium particle temperature which may even initiate the crystallization of nanoparticles.

The temperature of microparticles confined in a low-pressure rf-plasma was determined and the related energy balance of the particles has been studied. A suitable phosphor material has been found, showing temperature sensitive features which can be used for temperature measurement in plasma. Using microparticles made of this material, systematic measurements of the particle temperature have been performed with high resolution. To that purpose, the discharge power has been varied in argon and hydrogen was added to the discharge under low pressure conditions. Moreover, the applicability of the particles as a calorimetric probe was demonstrated. A simple balance model has been used to describe the most important energy fluxes between the particle and the surrounding plasma environment. It was possible to give a consistent description of the energy fluxes between plasma and immersed particles, which finally determine the particle temperature.

Because of the most probable electron impact dissociation the density of hydrogen atoms was assumed to be proportional to the electron density. The different contributions to particle heating deduced from the balance for the investigated gas mixture show a dominant role of recombination processes where free electrons and ions recombine at the particle surface which is approximately 70% of the heating source. The recombination of dissociated hydrogen delivers about 20% to the total energy influx. The remaining kinetic contributions

of electrons and ions are comparably small. As a result from the energy balance, the amount of atomic hydrogen can be estimated indirectly if its value for the sticking probability at the particle surface is estimated.

Combination of simultaneous electrical (e.g. charge) and calorimetric (e.g. temperature) measurements for the same particles (substrate material) in future experiments would be of interest, because both quantities are determined by the same physical processes. These experiments could provide valuable experimental data and lead to a deeper understanding of plasma-particle interactions.

References

[1] S. D. Bernstein, T. Y. Wong and R. W. Tustison, J. Vac. Sci. Technol. A **17** (2), pp. 571–576 (1999).

[2] H. Kersten, H. Deutsch, H. Steffen, G.M.W. Kroesen, R. Hippler, Vacuum **63**(2001), 385-431.

[3] J. G. Han, J. Phys. D Appl. Phys. **42** (4), p. 043001 (2009).

[4] A. von Keudell, Plasma Sources Sci. T. **9** (4), p. 455 (2000).

[5] B. Window, Surf. Coat. Tech. **71** (2), pp. 93 – 97 (1995).

[6] A. V. Gavrikov, A. S. Ivanov, A. F. Pal, O. F. Petrov, A. N. Ryabinkin,
A. O. Serov, Y. M. Shulga, A. N. Starostin and V. E. Fortov, AIP conf. proc. **1041**, pp. 237–238. AIP (2008).

[7] P. R. i Cabarrocas, N. Chabane, A. V. Kharchenko and S. Tchakarov, Plasma Phys. Contr. F. **46** (12B), p. B235 (2004).

[8] P. R. i Cabarrocas, Y. Djeridane, T. Nguyen-Tran, E. V. Johnson, A. Abramov
and Q. Zhang, Plasma Phys. Contr. F. **50** (12), p. 124037 (2008).

[9] P. R. i Cabarrocas, P. Gay and A. Hadjadj, J. Vac. Sci. Technol. A **14**, pp. 655–659 (1996).

[10] T. Ishigaki, T. Sato, Y. Moriyoshi and M. I. Boulos, J. Mater. Sci. Lett.**14** (23), pp. 1694–1697 (1995).

[11] H. Kersten, H. Deutsch, E. Stoffels, W. W. Stoffels and G. M. W. Kroesen, Int. J. Mass Spectrom. **223-224**, pp. 313 – 325 (2003).

[12] H. Kersten, H. Deutsch, E. Stoffels, W. W. Stoffels, G. M. W. Kroesen and R. Hippler, Contrib. Plasm. Phys. **41** (6), pp. 589–609 (2001).

[13] U. Kortshagen, J. Phys. D Appl. Phys. **42** (11), p. 113001 (2009).

[14] E. Stoffels, W. W. Stoffels, G. Ceccone, R. Hasnaoui, H. Keune, G. Wahl and F. Rossi, J. Appl. Phys. **86** (6), pp. 3442–3451 (1999).

[15] L. Mangolini, U. Kortshagen, Phys. Rev. E **79** (2009), 026405.

[16] I. Levchenko, S. Y. Huang, K. Ostrikov, and S. Xu, Nanotechnology **21**, 025605 (2010).

[17] I. Levchenko, K. Ostrikov, and D. Mariotti, Carbon **47**, 344 (2009).

[18] Z. L. Tsakadze, I. Levchenko, K. Ostrikov, and S. Xu, Carbon **45**, 2022 (2007).

[19] S. Sriraman, S. Agarwal, E. S. Aydil, and D. Maroudas, Nature (London) **418**, 62 (2002).

[20] M. Wolter, I. Levchenko, H. Kersten, K. Ostrikov, Appl. Phys. Lett. 96 (2010), 133105.

[21] J. Beckers, W. W. Stoffels and G.M.W. Kroesen, J. Phys. D: Appl. Phys. **42** (2009) 155206.

[22] R. Basner, F. Sigeneger, D. Loffhagen, G. Schubert, H. Fehske and H. Kersten, New J. Phys. **11** (2009) 013041.

[23] U. Kortshagen, J. Phys. D: Appl. Phys. **42** (2009) 113001.

[24] J. Goree, *Plasma Sources Sci. Technol.* **3 (1994)** 400.

[25] T. Matsoukas, M. Russel, *J. Appl. Phys.* **77 (1995)** 4285.

[26] V.A. Schweigert, I.V. Schweigert, *J. Phys. D: Appl. Phys.* **29 (1996)** 655.

[27] T. Matsoukas, *J. Colloid Interface Sci.* **187 (1997)** 474.

[28] G.S. Selwyn, K.L. Haller, E.F. Patterson, *J. Vac. Sci. Technol.* A **11 (1993)** 1132.

[29] G.S. Selwyn, J.E. Heidenreich, K.L. Haller, *Appl. Phys. Lett.* **57 (1990)** 1876.

[30] L. Boufendi, A. Bouchoule, Plasma Sources Sci. Technol. **3** (1994) 262.

[31] A. Bouchoule, L. Boufendi, Plasma Sources Sci. Technol. **2 (1993)** 204.

[32] M. Wolter, M. Hundt, H. Kersten, Vacuum (2010) doi:10.1016/j.vacuum.2010.01.016.

[33] H.R. Maurer, M. Hannemann, R. Basner, H. Kersten, Phys. Plasmas **17** (2010), 113707.

[34] H.R. Maurer, R. Basner, H. Kersten, Contrib. Plasma Phys. **50** (2010), 954.

[35] A. Bapat, C. Anderson, C.R. Perrey, C.B. Carter, S.A. Campbell, U. Kortshagen, *Plasma* Phys. Controlled Fusion **46** (2004) B97–109.

[36] J. E. Allen, Phys. Scripta **45** (5), pp. 497–503 (1992).

[37] C. Arnas and A. A. Mouberi, J. Appl. Phys. **105** (6), 063301 (2009).

[38] F. Galli and U. Kortshagen, IEEE T. Plasma Sci. **38** (4), pp. 803 –809 (2010).

[39] R. Piejak, V. Godyak, B. Alexandrovich and N. Tishchenko, Plasma Sources Sci. T. **7** (4), pp. 590–598 (1998).

[40] F. X. Bronold, H. Fehske, H. Kersten and H. Deutsch, Contrib. Plasm. Phys. **49** (4-5, Sp. Iss. SI), pp. 303–315 (2009).

[41] S. A. Khrapak and G. E. Morfill, Phys. Plasmas **13** (10), 104506 (2006).

[42] E. Stoffels, W. W. Stoffels, H. Kersten, G. H. P. M. Swinkels and G. M. W. Kroesen, Phys. Scripta **2001** (T89), p. 168 (2001).

[43] J. E. Daugherty and D. B. Graves, J. Vac. Sci. Technol. A **11** (4), pp. 1126–1131 (1993).

[44] H. Maurer, R. Basner and H. Kersten, Rev. Sci. Instrum. **79** (9), 093508 (2008).

[45] H. Maurer, R. Basner and H. Kersten, Plasmas. AIP Conf. Proc. **1041**, pp. 283–284. AIP (2008).

[46] D. Oliver and R. Enikov, Vacuum **58** (2-3), pp. 244 – 249 (2000).

[47] G. Swinkels, H. Kersten, H. Deutsch and G. M. W. Kroesen, J. Appl. Phys. **88** (4), pp. 1747 – 1755 (2000).

[48] M. Stahl, T. trottenberg, H. Kersten, Rev. Sci. Instrum. **81** (2010), 023504.

[49] H. T. Do, H. Kersten and R. Hippler, New J. Phys. **10** (5), p. 053010 (2008).

[50] D. Lee, L. Oksuz and N. Hershkowitz, Phys. Rev. Lett. **99** (15), p. 155004 (2007).

[51] W. Bleakney, Phys. Rev. **40** (4), pp. 496–501 (1932).

[52] B. Darwent, Bond Dissociation Energies in Simple Molecules. (1970).

[53] Y. Ralchenko, A. Kramida, J. Reader and N. A. Team: NIST Atomic Specta Database. NIST Atomic Spectra Database (version 3.1.5), [Online], (2008).

[54] P. C. Cosby and H. Helm, Chemical Physics Letters **152** (1), pp. 71 – 74 (1988).

[55] J. Lorenzen, H. Hotop, M. W. Ruf and H. Morgner, Zeitschrift für Physik A Hadrons and Nuclei **297** (1), pp. 19 – 23 (1980).

[56] E. Neyts, M. Yan, A. Bogaerts and R. Gijbels, J. Appl. Phys. **93** (9), pp. 5025–5033 (2003).

[57] M. Tatanova, G. Thieme, R. Basner, M. Hannemann, Y.B. Golubovskii, H. Kersten, Plasma Sources Sci. Technol. **15** (2006)8, 507

[58] J. Didierjean, S. Forget, S. Chenais, F. Druon, F. Balembois, P. Georges, K. Altmann, C. Pflaum, Proceedings of SPIE **5707** (2005), 370-379

[59] B. P. Lavrov, N. Lang, A. V. Pipa and J. Röpcke, Plasma Sources Sci. T. **15** (1), p. 147 (2006).